CHEMISTRY OF MATERIALS

Article

pubs.acs.org/cm

$NH_2CH{=}NH_2PbI_3$: An Alternative Organolead Iodide Perovskite Sensitizer for Mesoscopic Solar Cells

Shuping Pang,[†,#] Hao Hu,[†,#] Jiliang Zhang,[‡] Siliu Lv,[†] Yaming Yu,[§] Feng Wei,[⊥] Tianshi Qin,[∥] Hongxia Xu,[†] Zhihong Liu,[†] and Guanglei Cui*[,†]

[†]Qingdao Key Lab of Solar Energy Utilization and Energy Storage Technology, Qingdao Institute of Bioenergy and Bioprocess Technology, Chinese Academy of Sciences, Qingdao 266101, People's Republic of China

[‡]Department of Physics and Materials Science, City University of Hong Kong, Hong Kong SAR

[§]College of Materials Science and Engineering, Huaqiao University, Xiamen 361021, People's Republic of China

[⊥]General Research Institute for Nonferrous Metals, Beijing 100088, People's Republic of China

[∥]Ian Wark Laboratory, CSIRO Materials Science & Engineering, Clayton South, Victoria 3168, Australia

Supporting Information

ABSTRACT: A new nearly cubic $NH_2CH{=}NH_2PbI_3$ ($FAPbI_3$) perovskite was synthesized for the mesoscopic solar cells. The measured band gap of bulk $FAPbI_3$ is 1.43 eV and it is therefore potentially superior than the $CH_3NH_3PbI_3$ ($MAPbI_3$) as the light harvester. A homogeneous $FAPbI_3$ perovskite layer was deposited on the TiO_2 surface by utilizing the in situ dipping technology. As a result, a high efficiency of 7.5% was achieved using P3HT as the hole transport material. The nearly cubic crystal structure and appropriate band gap render this new $FAPbI_3$ perovskite extremely attractive for next generation high-efficiency low-cost solar cells.

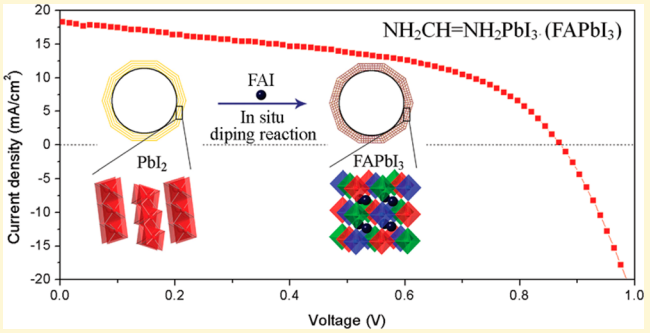

1. INTRODUCTION

It has been recognized that solar energy is one of the promising resources of renewable energy to power our lives. Compared with conventional crystalline silicon cell, thin film solar cell technology promises to reduce the cost of light-to-electricity conversion by using abundant materials and easy fabrication procedures.[1,2] A variety of promising light absorbing materials has been explored in both organic and inorganic systems. Generally, organic materials suffer from short lifetime for their degradation when exposed to light for a long time,[3,4] and the inorganic absorbers (e.g., quantum dots, QD) require a complicated synthetic procedure to satisfy the solution processing requirement.[5−7]

Recently, due to the high processability, large optical absorption cross section and excellent thermal stability, organolead halid perovskites ($APbX_3$) have become one of the most promising light harvesters for mesoscopic solar cells.[8−22] More and more new efficiency records of perovskite based solar cells have been achieved at rather short intervals. Up to now, a record efficiency of ∼15% has been achieved by solution processed $MAPbI_3$ (MA: $CH_3NH_3^+$) containing perovskite solar cells.[22] The optical absorption coefficient of $MAPbI_3$ is about 1.5×10^4 cm^{-1} at 550 nm and thermally stable up to 300 °C.[9,11,23] In the $MAPbI_3$ perovskite structure, the larger MA cation and the smaller Pb cation are, respectively, coordinated to twelve and six I anions, and PbI_6 octahedra are corner-shared to form a three-dimensional framework. The electronic properties of Pb halide perovskites are strongly dependent on the geometry of the three-dimensional network of the PbX_6 octahedra.[23] The measured band gap of $MAPbI_3$ is 1.51 eV at room temperature, which is higher than the optimized band gap value (1.40 eV) according to the Shockley−Queisser limit curve for a single band gap solar cell.[24]

To tune the band gap, one attempt is to substitute I with Br or Cl anions, resulting in the band gaps changed from 1.51 to 2.22 or 3.62 eV, respectively.[13] Such a modification is unfavorable for a wide range of light harvesting. Another strategy is to substitute the A site cations because the band gap of the perovskite is very sensitive to any modification (enlargement, tilting, and/or deformation) of the octahedra network.[25] It is known that, at room temperature, $MAPbI_3$ perovskite is a tetragonal rather than a cubic structure due to the smaller size of methylammonium cation ($CH_3NH_3^+$) according to the tolerance factor $f = (r_B + r_X)/\sqrt{2}(r_A + r_X)$.[23,25] The substitution of A site with a larger cation is thus expected to yield a higher symmetry of the perosvskite structure and a decrease of the band gap as well. However, the replacement of $CH_3NH_3^+$ with a long chain ethylammonium cation ($CH_3CH_2NH_3^+$) produces a layered perovskite crystalline structure with a band gap increased to 2.2 eV.[26] The failed

Received: December 6, 2013
Revised: January 13, 2014
Published: January 21, 2014

   dx.doi.org/10.1021/cm404006p | Chem. Mater. 2014, 26, 1485−1491

formation of the three-dimensional framework should be owed to the oversize $CH_3CH_2NH_3^+$cation. Therefore, it is logically feasible to employ an organic amine cation that is smaller than $CH_3CH_2NH_3^+$ but larger than $CH_3NH_3^+$ in size to fill the A site. A formamidinium cation ($HC(NH_2)_2^+$) with three atoms (excluding hydrogen) is smaller than that of $CH_3CH_2NH_3^+$ but larger than $CH_3NH_3^+$.[25,27]

In this paper, we have, for the first time, employed $HC(NH_2)_2^+$ to substitute $CH_3NH_3^+$ to synthesize the pure $FAPbI_3$ perovskite and subsequently study its photoelectrochemical properties as sensitizer in mesoscopic solar cells. It is demonstrated that the synthesized $FAPbI_3$ possesses a band gap of 1.43 eV and its corresponding absorption edge reaches 870 nm, which is superior to $MAPbI_3$ (820 nm) to serve as a light harvester.[11] It is noteworthy that the in situ dipping technology is more adoptable to synthesize the high-quality $FAPbI_3$ crystals upon a mesoporous TiO_2 scaffold at a lower processing temperature compared with a one-step spin-coating method. With poly(3-hexylthiophene) (P3HT) as the hole transport material (HTM) and a gold back contact, a power conversion efficiency of 7.5% with an open circuit voltage of 0.84 V and short circuit current of 18.3 mA/cm^2 was obtained. Considering its nearly cubic crystal structure and appropriate band gap, there still remains big room for further improvement of the $FAPbI_3$ solar cells through optimizing the $FAPbI_3$ thickness and crystallinity and also employing new hole transport materials.

2. EXPERIMENTAL SECTION

2.1. Synthesis of FAI. FAI was first prepared by directly mixing 3 g of formamidine acetate and 8.2 g of HI (45 wt % in water) at 0 °C for 2 h. The precipitate was collected by rotary drying at 65 °C for 30 min, which was followed by washing with a mixture of ethanol and diethyl ether by air pump filtration. The white solid was finally dried at 60 °C under vacuum for 2 days.

2.2. Synthesis of Bulk $FAPbI_3$ Peroviskite. $FAPbI_3$ perovskite powder sample was prepared by a solution method. The mixture of PbI_2 and FAI with a mole ratio of 1:1 was first dissolved in γ-butyrolactone (GBL) to form a 40 wt % solution. $FAPbI_3$ perovskite powder sample was prepared via evaporating the GBL solvent at 180 °C for 10 min on a glass substrate.

2.3. Electronic Structure Calculations. The electronic structure calculations were performed using the first-principles pseudopotential based density functional theory as implemented in the SIESTA package.[28,29] This software employs a localized orbital basis in the representation of wave functions. The double-ζ polarized numerical atomic orbital basis set is adopted to provide sufficient accuracy, and the core electrons are represented by norm-conserving pseudopotentials and the Perdew−Berke−Emzerhof exchange correlation energy within the generalized gradient approximation.[30] In the calculation, $HC(NH_2)_2^+$ was ignored and a uniform background charge density was added to neutralize the charge.

2.4. Synthesis of TiO_2 Gel. The TiO_2 dense layer was prepared using a sol−gel procedure.[31] 10 mL of titanium(IV) isopropoxide was mixed with 50 mL of 2-methoxyethanol and 5 mL of ethanolamine in a three-necked flask each connected with a condenser, thermometer, and argon gas inlet/outlet. Then, the mixed solution was heated to 80 °C for 2 h under magnetic stirring, followed by heating to 120 °C for 1 h. The two-step heating was then repeated for two times to prepare a viscous solution.

2.5. Solar Cell Fabrication and Characterization. Fluorine-doped tin oxide (FTO) coated glass was patterned by etching with Zn powder and 1 M HCl diluted in Milli-Q water. The etched substrate was then cleaned with ethanol, saturated KOH solution in isopropanol, and water and then dried with clean dry air. Subsequently, a 30 nm thick dense TiO_2 layer was fabricated from TiO_2 gel as described above. After a treatment with heat at 500 °C for 30 min, a 500 nm thick TiO_2 porous layer was fabricated on the TiO_2 dense layer from a dilute commercial TiO_2 paste (1:2.5 with ethanol by weight) at 3000 rpm. The layers were then sintered in air at 550 °C for 30 min. For the one-step solution processed solar cells, a thin $FAPbI_3$ perovskite layer was formed by spin-coating of 40 wt % PbI_2:FAI mixture in *N,N*-dimethylformamide (DMF). To get a pure $FAPbI_3$ perovskite phase, the mole ratio of PbI_2 to FAI was modified to 1:1.5. For the solar cells fabricated using the in situ dipping technology, PbI_2 powder was first dissolved in DMF solution to form a 0.8 M solution and then spin-coated (3000 rpm) on the mesoporous TiO_2 film to prepare a FTO/TiO_2/PbI_2 structure.[22] The in situ reaction was carried out by directly dipping the FTO/TiO_2/PbI_2 substrate into an isopropanol solution containing 5 M FAI until the PbI_2 film became dark brown, followed by a heating treatment at 100 °C for 10 min. The HTM (1,2-dichlorobenzene solution containing 10 mg/mL P3HT) was cast onto the perovskite coated substrate and spun at a rate of 1500 rpm for 60 s. Finally, a 60 nm Au electrode was thermally evaporated to complete the solar cells. J−V characteristics were measured (2400 Series Source Meter, Keithley Instruments) under simulated AM 1.5G sunlight at 100 mW/cm^2. The area of the perovskite solar cells were typically 0.15 cm^2. External quantum efficiency (EQE) measurements were carried out on a Newport setup comprising a Xe lamp, a monochromator, a current−voltage preamplifier, and a lock-in amplifier. It is worth noting that all the device fabrication and measurement is under ambient conditions at a relative humidity of 30−40%. The characterization of the materials was summarized in the Supporting Information.

3. RESULTS AND DISCUSSION

To synthesize $FAPbI_3$, the formamidine iodide ($HC(NH_2)_2I$, FAI) was first prepared by directly mixing formamidine acetate and hydroiodic acid (HI) at 0 °C. The elemental analysis shows the weight ratio of C:N:H:I in the as-prepared FAI is 7.00:16.33:2.99:73.68, which is in very good agreement with theoretical atomic ratio of 1:2:5:1(C:N:H:I).The ^{1}H and ^{13}C nuclear magnetic resonance (NMR) of the white powder were further characterized to verify the purity of the FAI (see Supporting Information, Figure S1−2). The FAI is very pure with no presence of any impurity. Subsequently, the black $FAPbI_3$ powder sample was prepared by the solution method. It was found that the mixture of PbI_2 and FAI with a mole ratio of 1:1 was soluble in DMF and GBL. In this paper, bulk $FAPbI_3$ sample was prepared via drying GBL solution at 180 °C on glass or quartz substrates. For the construction of the $FAPbI_3$ solar cells, thin $FAPbI_3$ perovskite layers were formed by one-step solution processing and two-step dipping technology, respectively, which will be described in details later.

The $FAPbI_3$ powder on the glass substrate was characterized by powder X-ray diffraction (XRD) on a Bruker-AXS Microdiffractometer with Cu Kα radiation at room temperature, as shown in Figure 1. The sharp diffraction peaks indicate

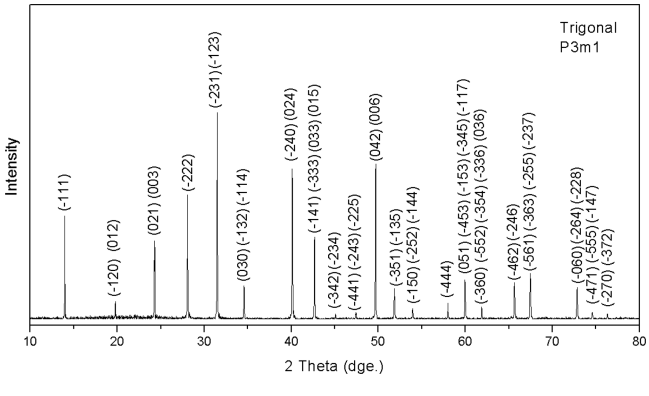

Figure 1. Typical XRD pattern of the $FAPbI_3$ film on a glass substrate.

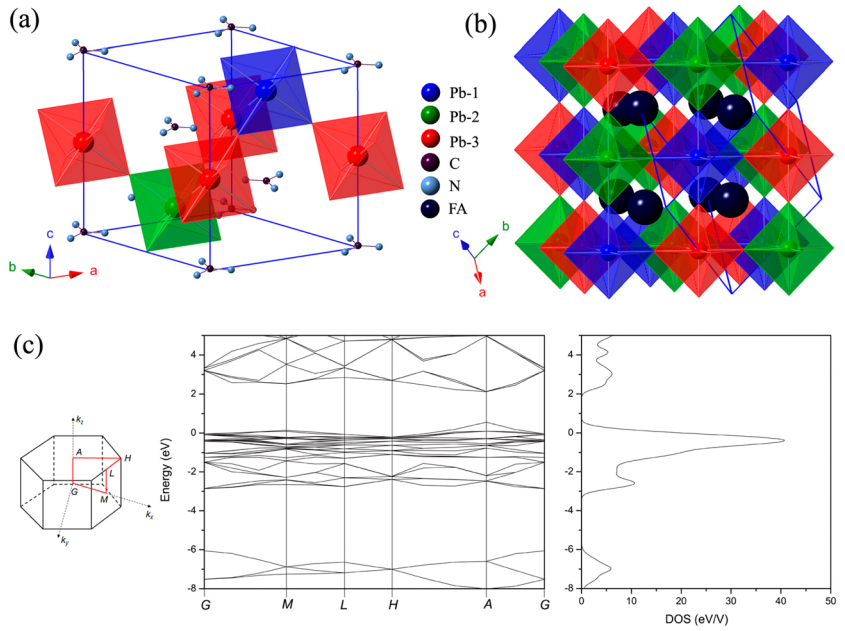

Figure 2. (a) Primitive unit cell of the trigonal crystal structure of $FAPbI_3$. (b) The cubic structure with a slight distortion when ignoring the displacement and orientation of $HC(NH_2)_2^+$ cations. (c) The schematic brillouin zone, calculated band structure and electronic density of states for the $FAPbI_3$, respectively. The Fermi level is chosen as the energy reference at 0 eV.

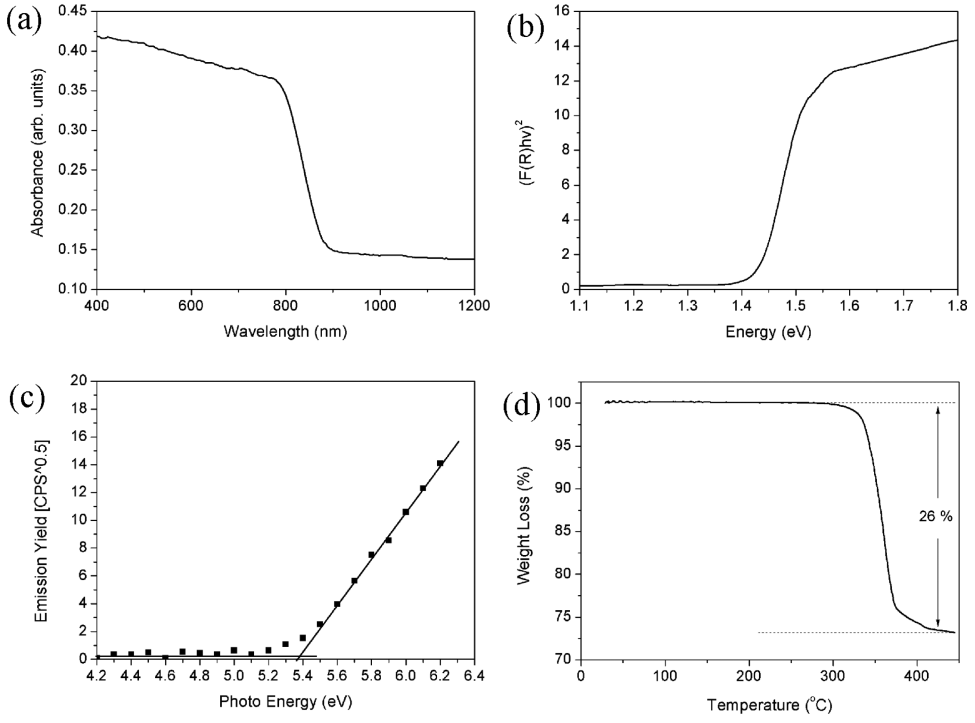

Figure 3. Optical, electronic and thermal properties of the $FAPbI_3$. (a, b) UV−vis/NIR absorption spectrum and transformed Kubelka−Munk spectrum of $FAPbI_3$ film that was formed by drop casting on a quartz substrate of the GBL solution containing PbI_2 and FAI with a mole ratio of 1:1 and then annealled at 180 °C for 10 min, respectively. (c) Photo electron spectroscopy in air (PESA) of $FAPbI_3$ film on glass substrate. (d) Weight loss as a function of temperature.

the high crystallinity of the as-synthesized $FAPbI_3$ compound. Rietveld refinement analysis of the X-ray powder diffraction pattern indicates that the synthesized $FAPbI_3$ is a pure phase with the space group of $P3m1$ (Supporting Information, Figure S3),[32] which was in good agreement with the very recent report.,[33] A point worth emphasizing is, under our experimental condition (section 2), that no decomposition of the formamidine was found. The high quality of the $FAPbI_3$ yields the possibility to exactly study its photoelectric properties in mesoscopic solar cells.

In the ideal cubic $Pm\bar{3}m$ structure of ABX_3 perovskites, the single A atom (such as Cs) could occupy the position in the center of the cube of the perovskite structure. In the case of $HC(NH_2)_2^+$, this is not possible in this space group because the

dx.doi.org/10.1021/cm404006p | Chem. Mater. 2014, 26, 1485−1491

$HC(NH_2)_2^+$ cations tend to be disordered in the cuboctahedral cages formed by 12 nearest-neighbor iodine atoms from the PbI_6^{4-} octahedra.[25] As a result, the synthesized $FAPbI_3$ adopts the *P3m*1 trigonal space group with lattice parameter of a = 9.0008(8) Å, b = 9.0008(8) Å, c = 11.012(2) Å, and α = 90°, β = 90°, γ = 120° (Figure 2a), according to the Rietveld refinement. When the effect of $HC(NH_2)_2^+$ on the symmetry of crystal lattice was ignored, the $FAPbI_3$ could then be regarded as a nearly cubic structure, as shown in Figure 2b. The tiny change of Pb−I bonds length (3.169−3.181 Å) in PbI_6 octahedra also supports its close relationship with the cubic structure, whereas in the tetragonal distortion of cubic $MAPbI_3$, the Pb−I bonds length varies from 3.156 to 3.213 Å.[33] It has been reported that the electronic properties of such compounds are strongly dependent on the inorganic framework.[23,25] At this point, the band gap of $FAPbI_3$ should be close to that of their ideal cubic $MAPbI_3$. On the basis of the data obtained by the Rietveld refinement, band structure and density of states (DOS) were theoretically calculated for $FAPbI_3$ perovskite as shown in Figure 2c.[30,34] The electronic band structure along the high-symmetry k lines and the projected density of states show that $FAPbI_3$ has a well-defined direct band gap of 1.50 eV at A (0, 0, 1/2).

In Figure 3a, the transmittance spectrum shows the strong absorption of the light with the wavelength shorter than 870 nm. The diffuse reflectance spectrum (SSI) and the transformed Kubelka−Munk spectrum for the $FAPbI_3$ powder were presented in Figure 3b. The optical absorption coefficient (α) is calculated using reflectance data according to the Kubelka−Munk equation, $F(R) = \alpha = (1 - R)^2/2R$, where R is the percentage of reflected light.[35] The incident photon energy ($h\nu$) and the optical band gap (Eg) are related to the transformed Kubelka−Munk function, $F(R)h\nu^p = A(h\nu - Eg)$, where A is the constant and p is the power index that is related to the optical absorption. Similar to $MAPbI_3$, there is a obvious "cut-off" feature in the UV−vis/NIR absorption spectrum, indicating the $FAPbI_3$ is also a direct band gap semiconductor. The measured band gap is ~1.43 eV from the extrapolation of the liner part of $F(R)h\nu^2$ plot, coinciding well with the theoretical calculation. The absorption edge reaches 870 nm, which is about 30 nm wider than that of the $MAPbI_3$ measured under the same condition. The extended absorption edge could bring ~6% more light absorption according to the standard solar spectrum. The measured valence band (VB) of $FAPbI_3$ film on a glass substrate by Photo Electron Spectroscopy in air (PESA)[36] was −5.38 eV and from the observed optical band gap, the conduction band (CB) of $FAPbI_3$ is calculated to be −3.95 eV. The thermogravimetric analysis result under an argon atomosphere in Figure 3d shows that the bulk sample was thermally stable up to 300 °C and he 26% weight loss was consistent with the complete decomposition to PbI_2 at 430 °C.

Similar to the previous reports about the $MAPbI_3$ solar cells, $FAPbI_3$ thin layer absorber was first fabricated by spin-coating a 40 wt % DMF solution of FAI and PbI_2 with a modified mole ratio (see section 2). Unlike the $MAPbI_3$ perovskite, the one-step spin-coated PbI_2:FAI film could not change to very dark under a 100 °C thermal annealing treatment, as shown in Figure S4 (Supporting Information). With the increase of the annealing temperature from 100 to 160 °C, the color of the FAI:PbI_2 changes to dark and then fade. The corresponding XRD patterns of these samples are shown in Figure 4c−f. For comparison, the XRD patterns of calculated $FAPbI_3$ perovskite and FTO/TiO_2 substrate are also presented in Figure 4a,b,

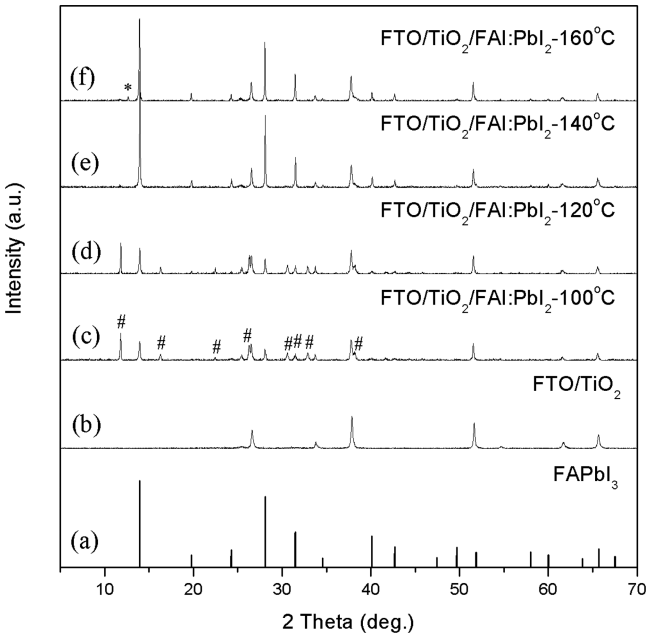

Figure 4. (a) Calculated XRD pattern of $FAPbI_3$. (b) The XRD pattern of the FTO/TiO_2 substrate. (c−f) The XRD patterns of the spin coated FAI:PbI_2 solution on the mesoporsous TiO_2 films and annealed at 100, 120, 140 and 160 °C for 30 min, respectively.

respectively. As shown in Figure 4c, with a 100 °C thermal treatment, only a low content of the $FAPbI_3$ perovskite was formed. Besides the peaks from the FTO/TiO_2 substrate and the $FAPbI_3$ perovskite, there are some additional diffraction peaks, as marked with "#", which attributes to the presence of a new yellow *P*63*mc* $FAPbI_3$ phase with layered crystal structure (Supporting Information, Figure S5).[28] With the annealing temperature increased to 120 °C, there is a little increase of the content of the $FAPbI_3$ perovskite according to the diffraction intensity. When the annealing temperature increased to 140 °C, almost all the diffraction peaks could be indexed to the $FAPbI_3$ perovskite (Figure 4e). With the temperature increased to 160 °C, there is some PbI_2 (*) appeared in the $FAPbI_3$ film.

The $FAPbI_3$ based solar cell was fabricated with P3HT as the HTM. The VB of $FAPbI_3$ is −5.38 eV below vacuum level, which is lower than that of P3HT (Figure 5a). For the device fabrication, the spin-coated FAI:PbI_2 was thermally annealed at 120, 130, 140 and 150 °C for 30 min, to serve as the light harvester, and P3HT was spin-coated on top of the perovskite layer. It was found that the solar cell annealed at around 140 °C delivered the highest efficiency as shown in Figure 5(b). An open-circuit voltage of 0.55 V and a short-circuit current density of 16.6 mA/cm^2 were achieved. The overall conversion efficiency is 3.7%, which is comparable to the $MAPbI_{3-x}Cl_x$ solar cell (3.8%) and lower than $MAPbI_3$ solar cell (6.7%) also using P3HT as the HTM.[19,37] There are many reasons responsible for the relatively poor performance, such as the unoptimized film thickness and spin-coating condition. Another very important reason is proposed to the relatively high annealing temperature, which may result in a poor crystal quality for the formation of more defects in the perovskite layer. The same result was also found in the literature.[9]

In previous reports concerning the lead iodide perovskite solar cells, the perovskite quantum-dots were crystallized out from the solvents such as GBL and DMF, resulting in low coverage on the TiO_2 surface. The two-step solid-solution

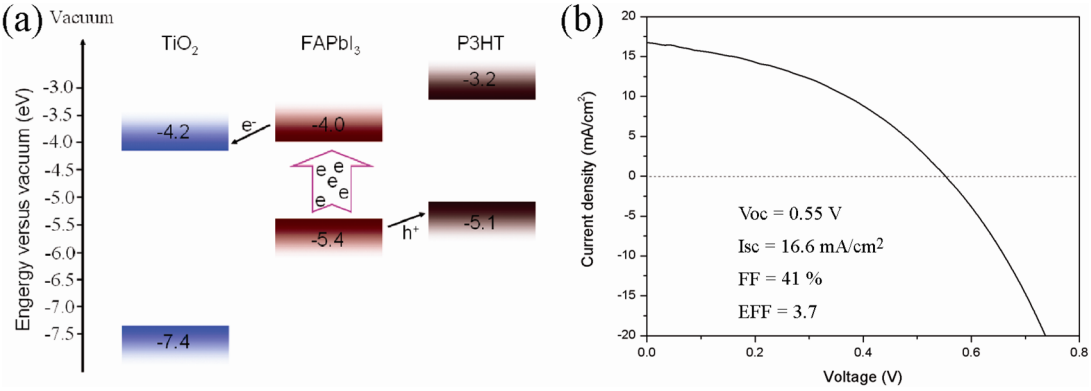

Figure 5. (a) Schematic energy level diagram of TiO_2, $FAPbI_3$ and P3HT. (b) The photocurrent density–voltage (J–V) curve of the spin coated $FAPbI_3$ solar cells with an efficiency of 3.7%.

process for the $MAPbI_3$ as shown in Figure 6 could obviously enhance the solar cell performance.[22,38] Another advantage is

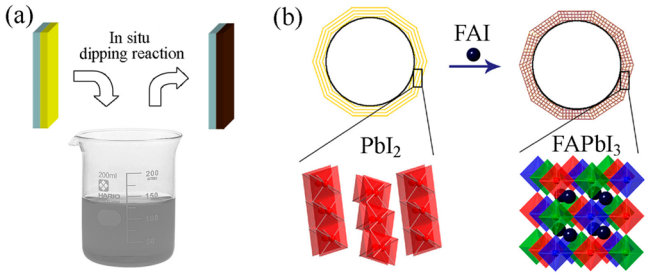

Figure 6. (a) Schematic illustration of in situ formation of $FAPbI_3$ by in situ dipping reaction of PbI_2 and FAI on the TiO_2 surface.

that such an in situ dipping technique could also decrease the reaction temperature. This is especially important for the $FAPbI_3$ based solar cells. In a typical procedure, a PbI_2 solution was first spin-coated on a mesoporous TiO_2 film to produce a $FTO/TiO_2/PbI_2$ structure with a bright yellow color. Then the $FTO/TiO_2/PbI_2$ substrate was dipped in a dilute FAI solution. The reaction of solid PbI_2 and FAI solution was very fast. During the reaction, the color gradually changed from yellow to dark red. The complete reaction time highly depends on the thickness of the PbI_2 film and the concentration of the FAI. In our experimental conditions, a 1 min dipping time could get the pure phase as a nearly cubic $FAPbI_3$ perovskite film, as shown in the optical images in Figure S6 (Supporting Information) and its corresponding XRD patterns in Figure S7 (Supporting Information). With increased dipping times, the color of the film changed from yellow (PbI_2) to dark ($FAPbI_3$ perovskite) and then faded. This phenomenon is in agreement with the published results.[28] Therefore, the control of the dipping time is of great importance for the $FAPbI_3$ based mesoscopic solar cells.

As above-mentioned, such a two-step dipping reaction could directly form a dark red layer even without additional thermal treatment as shown in Figure 7a. The transmission electron microscopy (TEM) image (Figure 7b) of the $TiO_2/FAPbI_3$ sample scratched from the mesoporous film reveals the formation of the $FAPbI_3$ perovskite thin film on the TiO_2 surface, which is much different from the $MAPbI_3$ quantum dots structure prepared from the one-step spin-coating technique from the GBL solution. After the in situ dipping reaction, as shown in Figure 7c,d, there are still many $FAPbI_3$

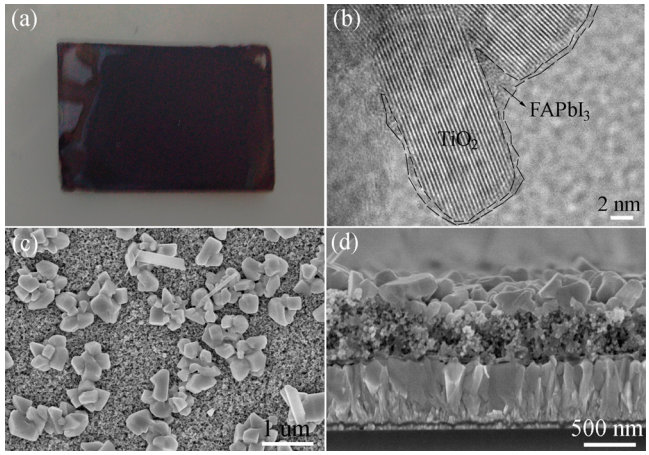

Figure 7. (a) Schematic illustration of in situ formation of $FAPbI_3$ by in situ dipping reaction of PbI_2 and FAI on the TiO_2 surface. (b) HRTEM image of the $FAPbI_3$ continuously covered on the mesoporous TiO_2 film. (c, d) Surface and cross-section SEM images of $FAPbI_3/TiO_2$ film.

domains on the mesoporous TiO_2 surface. The large $FAPbI_3$ particles are of polyhedron structure with the size of ~0.5–1 μm. The cross-section scanning electron microscopy (SEM) image in Figure 7d and the EDS mapping for titanium, lead, and iodine in Figure S8a–d (Supporting Information) further indicate that the homogeneous reaction of PbI_2 and FAI throughout the whole mesoporous TiO_2 layer and the $FAPbI_3$ are both located in the mesopores and top-surface of the mesoporous TiO_2 layer.

The phase purity of the $FAPbI_3$ formed via the two-step dipping reaction was studied by XRD, as shown in Figure 8, which is in very good agreement with the calculated XRD powder pattern of $FAPbI_3$. The two-step dipping reaction followed by a 100 °C thermal annealing treatment could efficiently form a pure phase nearly cubic $FAPbI_3$ perovskite crystal structure. The lower temperature processing feasibility is one of the huge advantages of the two-step dipping technique over the one-step spin-coating method.

After the in situ dipping reaction and thermal annealing treatment of $FAPbI_3$ layer at 100 °C for 10 min, 10 mg/mL of P3HT in 1,2-dichlorobenzene was spin-coated on the $FAPbI_3$ film at 1500 rpm. Then a 60 nm thick Au electrode was evaporated on the top of P3HT through a shadow mask. Before spin-coating P3HT layer, the absorption spectra of $FTO/TiO_2/$

dx.doi.org/10.1021/cm404006p | Chem. Mater. 2014, 26, 1485–1491

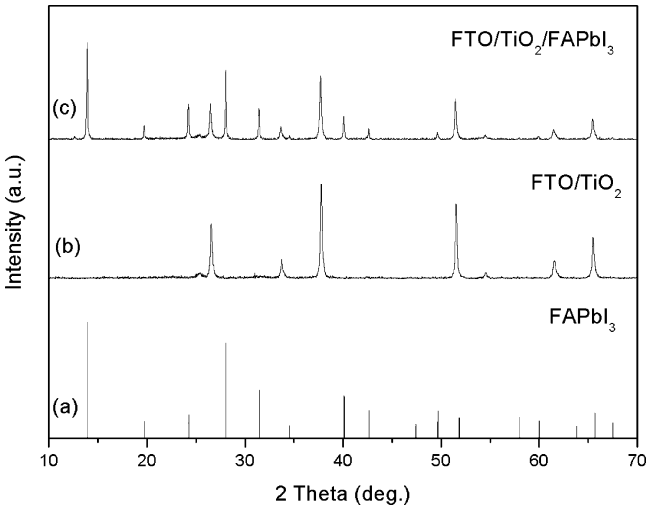

Figure 8. (a) Calculated XRD pattern of $FAPbI_3$. (b) The XRD pattern of the FTO/TiO_2 substrate. (c) The XRD pattern of the $FAPbI_3$ on the mesoporsous TiO_2 film synthesized by the in situ dipping technology and subsequently heated at 100 °C for 30 min.

$FAPbI_3$ and FTO/TiO_2 films were measured, as shown in Figure 9a. The $FAPbI_3$ perovskite in the mesoporous TiO_2 film shows an absorption edge at ∼820 nm. The blue shift of absorption edges of the $FAPbI_3$ perovskite in mesoporous TiO_2 (820 nm) than that on the glass substrate (870 nm, Figure 2a) is ascribed to the quantum size effect. Figure 9b presents the J−V curve for $FAPbI_3$ based solar cell. The power conversion efficiency of $FAPbI_3$ based solar cell reaches 7.5%, with an open-circuit voltage of 0.84 V and a short-circuit current density of 18.3 mA/cm^2. It is proposed that there are two reasons responsible for the improvement of the power conversion efficiency based on the in situ dipping reaction over the one-step spin-coating technique. One is an improved loading of the $FAPbI_3$ in the holes of meso-porous layer.[22] Another reason is the relatively low annealing temperature of the $FAPbI_3$ film. Additionally, compared with the traditional $MAPbI_3$ based solar cell, the $FAPbI_3$ solar cell exhibits a very high current density.[22] Such improvement is due to its wider absorption range than the $MAPbI_3$ as shown in Figure S9. The $FAPbI_3$ will provide new opportunities for improving the efficiency of the perovskite solar cells.

4. CONCLUSIONS

In summary, a new $FAPbI_3$ adopts the *P3m*1 trigonal space group was synthesized and studied. The lattice parameters of the $FAPbI_3$ are of a = 9.0008(8) Å, b = 9.0008(8) Å, c = 11.012(2) Å, and α = 90°, β = 90°, γ = 120°. Therefore, the new compound could be considered as a nearly cubic perovskite structure with a slight distortion when ignoring the displacement and orientation of $HC(NH_2)_2^+$ cations. The $FAPbI_3$ based solar cells were subsequently fabricated by one-step solution processing and two-step dipping technology, respectively. It was found that the two-step dipping technology was more favorable to achieve a relatively high efficiency due to feasibility of forming a phase-pure $FAPbI_3$ perovskite at relatively low temperaure (100 °C). The nearly cubic crystal structure and extended light absorbance render this new $FAPbI_3$ perovskite extremely attractive for the high efficient perovskite solar cells.

■ ASSOCIATED CONTENT

Supporting Information

NMR of the synthesized FAI, Pawley fit of the powder X-ray diffraction pattern of $FAPbI_3$, photographs of the spin-coated and thermally annealed PbI_2:FAI films, XRD pattern of the yellow phase $FAPbI_3$, photographs, XRD patterns, cross section SEM image, EDS maps and of $FAPbI_3$ films fabricated using the two-step method, EQE of the $FAPbI_3$ solar cells (PDF). This material is available free of charge via the Internet at http://pubs.acs.org.

■ AUTHOR INFORMATION

Corresponding Author

*G. C. E-mail: cuigl@qibebt.ac.cn.

Author Contributions

#All authors have given approval to the final version of the paper. These authors contributed equally.

Funding

This work was financially supported by the National Natural Science Foundation (No. 51202266, 21202178), Natural Science Foundation of Shandong Province(No.ZR2013FZ001) and National Program on Key Basic Research Project of China (973 Program) (No. MOST2011CB935700).

Notes

The authors declare no competing financial interest.

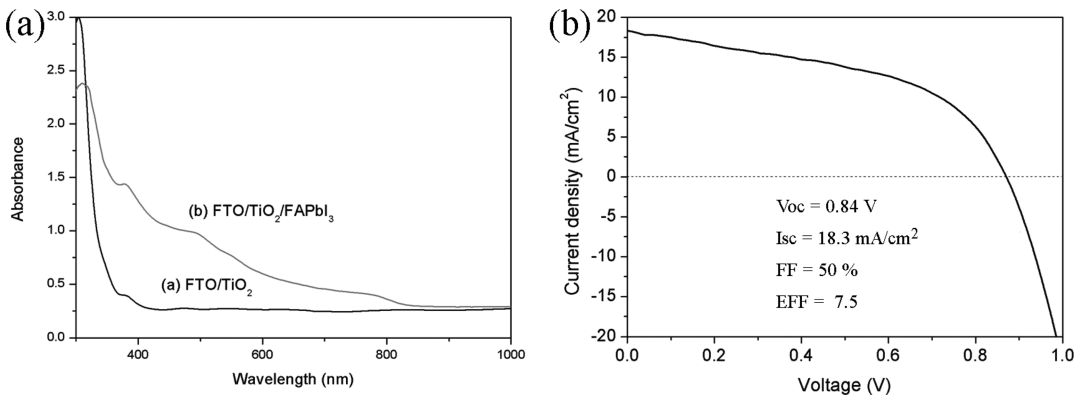

Figure 9. (a) UV−vis/NIR absorption spectra of FTO/TiO_2 and $FTO/TiO_2/FAPbI_3$ obtained by in situ dipping technology, respectively. (b) The J−V curve of the as-fabricated $FAPbI_3$ solar cells.

■ ACKNOWLEDGMENTS

We thank Dr. L. Chen of Max Planck Institute for Polymer Reasearch, Prof. R. Yang of Qingdao Institute of Bioenergy and Bioprocess Technology, Chinese Academy of Sciences, and Prof. G. Qin of Peking University for their kind and valuable discussion.

■ REFERENCES

(1) Congreve, D. N.; Lee, J. Y.; Thompson, N. J.; Hontz, E.; Yost, S. R.; Reusswig, P. D.; Bahlke, M. E.; Reineke, S.; Van Voorhis, T.; Baldo, M. A. *Science* **2013**, *340*, 334−337.
(2) Nozik, A. J.; Beard, M. C.; Luther, J. M.; Law, M.; Ellingson, R. J.; Johnson, J. C. *Chem. Rev.* **2010**, *110*, 6873−6890.
(3) Ecker, B.; Nolasco, J. C.; Pallares, J.; Marsal, L. F.; Posdorfer, J.; Parisi, J.; von Hauff, E. *Adv. Funct. Mater.* **2011**, *21*, 2705−2711.
(4) Wang, X. Z.; Zhao, C. X.; Xu, G.; Chen, Z. K.; Zhu, F. R. *Sol. Energy Mater.* **2012**, *104*, 1−6.
(5) Etgar, L.; Moehl, T.; Gabriel, S.; Hickey, S. G.; Eychmuller, A.; Gratzel, M. *ACS Nano* **2012**, *6*, 3092−3099.
(6) Rath, A. K.; Bernechea, M.; Martinez, L.; Konstantatos, G. *Adv. Mater.* **2011**, *23*, 3712−3717.
(7) Ip, A. H.; Thon, S. M.; Hoogland, S.; Voznyy, O.; Zhitomirsky, D.; Debnath, R.; Levina, L.; Rollny, L. R.; Carey, G. H.; Fischer, A.; Kemp, K. W.; Kramer, I. J.; Ning, Z. J.; Labelle, A. J.; Chou, K. W.; Amassian, A.; Sargent, E. H. *Nat. Nanotechnol.* **2012**, *7*, 577−582.
(8) Kojima, A.; Teshima, K.; Shirai, Y.; Miyasaka, T. *J. Am. Chem. Soc.* **2009**, *131*, 6050−6051.
(9) Im, J. H.; Lee, C. R.; Lee, J. W.; Park, S. W.; Park, N. G. *Nanoscale* **2011**, *3*, 4088−4093.
(10) Etgar, L.; Gao, P.; Xue, Z.; Peng, Q.; Chandiran, A. K.; Liu, B.; Nazeeruddin, M. K.; Gratzel, M. *J. Am. Chem. Soc.* **2012**, *134*, 17396−17399.
(11) Kim, H. S.; Lee, C. R.; Im, J. H.; Lee, K. B.; Moehl, T.; Marchioro, A.; Moon, S. J.; Humphry-Baker, R.; Yum, J. H.; Moser, J. E.; Gratzel, M.; Park, N. G. *Sci. Rep.* **2012**, *2*, 591.
(12) Lee, M. M.; Teuscher, J.; Miyasaka, T.; Murakami, T. N.; Snaith, H. J. *Science* **2012**, *338*, 643−647.
(13) Noh, J. H.; Im, S. H.; Heo, J. H.; Mandal, T. N.; Seok, S. I. *Nano Lett.* **2013**, *13*, 1764−1769.
(14) Ball, J. M.; Lee, M. M.; Hey, A.; Snaith, H. *Energy Environ. Sci.* **2013**, *6*, 1739−1743.
(15) Laban, W. A.; Etgar, L. *Energy Environ. Sci.* **2013**, *6*, 3249−3253.
(16) Jeng, J.-Y.; Chiang, Y.-F.; Lee, M.-H.; Peng, S.-R.; Guo, T.-F.; Chen, P.; Wen, T.-C. *Adv. Mater.* **2013**, *25*, 3727−3732.
(17) Cai, B.; Xing, Y.; Yang, Z.; Zhang, W.-H.; Qiu, J. *Energy Environ. Sci.* **2013**, *6*, 1480−1485.
(18) Edri, E.; Kirmayer, S.; Cahen, D.; Hodes, G. *J. Phys. Chem. Lett.* **2013**, *4*, 897−902.
(19) Abrusci, A.; Stranks, S. D.; Docampo, P.; Yip, H.-L.; Jen, A. K. Y.; Snaith, H. J. *Nano Lett* **2013**, *13*, 3124−3128.
(20) Bi, D. Q.; Yang, L.; Boschloo, G.; Hagfeldt, A.; Johansson, E. M. J. *J. Phys. Chem. Lett.* **2013**, *4*, 1532−1536.
(21) Qiu, J. H.; Qiu, Y. C.; Yan, K. Y.; Zhong, M.; Mu, C.; Yan, H.; Yang, S. H. *Nanoscale* **2013**, *5*, 3245−3248.
(22) Burschka, J.; Pellet, N.; Moon, S.-J.; Humphry-Baker, R.; Gao, P.; Nazeeruddin, M. K.; Gratzel, M. *Nature* **2013**, *499*, 316−319.
(23) Baikie, T.; Fang, Y. N.; Kadro, J. M.; Schreyer, M.; Wei, F. X.; Mhaisalkar, S. G.; Graetzel, M.; White, T. J. *J. Mater. Chem. A* **2013**, *1*, 5628−5641.
(24) Miller, O. D.; Yablonovitch, E.; Kurtz, S. R. *IEEE J. Photovoltaics* **2012**, *2*, 303−311.
(25) Borriello, I.; Cantele, G.; Ninno, D. *Phys. Rev. B* **2008**, *77*, 235214.
(26) Im, J.-H.; Chung, J.; Kim, S.-J.; Park, N.-G. *Nanoscale Res. Lett.* **2012**, *7*, 353.
(27) Mitzi, D. B.; Liang, K. *J. Solid State Chem.* **1997**, *134*, 376−381.
(28) Ordejón, P.; Artacho, E.; Soler, J. M. *Phys. Rev. B* **1996**, *53*, R10441.
(29) Soler, J. M.; Artacho, E.; Gale, J. D.; García, A.; Junquera, J.; Ordejón, P.; Sánchez-Portal, D. *J. Phys.: Condens. Matter* **2002**, *14*, 2745.
(30) Perdew, J. P.; Burke, K.; Ernzerhof, M. *Phys. Rev. Lett.* **1996**, *77*, 3865−3868.
(31) Cho, S.; Lee, K.; Heeger, A. J. *Adv. Mater.* **2009**, *21*, 1941−1944.
(32) Young, R. A.; Larson, A. C.; Paive-santos, C. O. *User's Guide to Program DBWS-9807a for Rietveld Analysis of X-ray and Newtron Powder Diffraction Patterns with a PC and Various Other Computers*; School of Physics, Georgia Institute of Technology: Atlanta, GA, 2000.
(33) Stoumpos, C. C.; Malliakas, C. D.; Kanatzidis, M. G. *Inorg. Chem.* **2013**, *52*, 9019−9038.
(34) Blochl, P. E.; Jepsen, O.; Andersen, O. K. *Phys. Rev. B* **1994**, *49*, 16223−16233.
(35) Lin, H.; Huang, C. P.; Li, W.; Ni, C.; Shah, S. I.; Tseng, Y. H. *Appl. Catal., B* **2006**, *68*, 1−11.
(36) Bronstein, H.; Frost, J. M.; Hadipour, A.; Kim, Y.; Nielsen, C. B.; Ashraf, R. S.; Rand, B. P.; Watkins, S.; McCulloch, I. *Chem. Mater.* **2013**, *25*, 277−285.
(37) Heo, J. H.; Im, S. H.; Noh, J. H.; Mandal, T. N.; Lim, C. S.; Chang, J. A.; Lee, Y. H.; Kim, H. J.; Sarkar, A.; Nazeeruddin, M. K.; Gratzel, M.; Seok, S. I. *Nat. Photonics* **2013**, *7*, 487−492.
(38) Liang, K. N.; Mitzi, D. B.; Prikas, M. T. *Chem. Mater.* **1998**, *10*, 403−411.